# A Westerbork survey of rich clusters of galaxies. III - Observations of the Coma Cluster at 610 MHz

Jaffe, W.J.; Valentijn, E.A.; Perola, G.C.

Astron. & Astrophys. 49, 179—192 (1976)

# A Westerbork Survey of Rich Clusters of Galaxies

## III. Observations of the Coma Cluster at 610 MHz

W. J. Jaffe
Sterrewacht, Leiden

G. C. Perola
Istituto di Scienze Fisiche and Laboratorio di Fisica Cosmica e Tecnologie Relative, Milano

E. A. Valentijn
Sterrewacht, Leiden

Received January 26, 1976

**Summary.** A WSRT full synthesis observation at 610 MHz of an area 1°.6 radius about the centre of the Coma Cluster of galaxies yielded the detection of twenty cluster members with $m_p \leqq 17.5$, doubling the number of those detected at 1415 MHz (Papers I and II). Eight of these are of elliptical or SO type, twelve are of spiral or irregular type (two are Markarian galaxies). The radio luminosity function LF above $P_{610}=2\times 10^{20}$ W Hz$^{-1}$ sterad$^{-1}$ is obtained separately for the (E+SO) and the (S+I) groups. No significant difference is found in the (E+SO) LF when compared with that obtained at 1415 MHz for a sample of five rich clusters (Paper II). The (S+I) galaxies appear slightly overluminous in radio with respect to the nearby field spirals. No significant dependence of the LF on the distance of the galaxies from the centre of the cluster is found. The spectral indexes $\alpha_{610}^{1415}$ and the presence of optical emission lines in the galaxies detected is briefly discussed. A probable correlation between the radio power and the presence of emission lines in the (S+I) galaxies is pointed out. Maps of the sources 5C4.81 and 85 and of the "halo" source surrounding them are presented. The steepening of the spectral index $\alpha_{610}^{1415}$ along the tail of 5C4.81 and the bend in the tail are discussed in the model of a radiogalaxy moving through the intracluster gas. The map of the low brightness "halo" source is obtained for the first time, confirming the conclusion reached by Willson (1970) on its truly diffuse nature. The measurements of the "halo" are affected by TV interference. After correcting for this, the visibility amplitude as a function of the baseline squared is obtained and fitted with a gaussian spherically symmetric brightness distribution of the type $\exp(-R^2/2a^2)$, with $a=12'\pm 2'$. This size is slightly less than those determined at lower frequencies.

**Key words:** clusters of galaxies — radio sources — luminosity function

### I. Introduction

This is the third in a series of papers on the radio properties of galaxies in nearby rich clusters. Paper I (Jaffe and Perola, 1975) described a 1415 MHz survey of 5 such clusters (A 1656, A 2147, A 2151, A 2197, A 2199) along with results of an optical identification search. Paper II (Jaffe and Perola, 1976) used these data to derive the radio luminosity function (LF) of the cluster galaxies.

We are reobserving these clusters at 610 MHz with the Westerbork Synthesis Radio Telescope (WSRT) in order to increase the number of galaxies surveyed in each cluster, due to the larger field of view of the telescope at this frequency, and to obtain spectral index information on the sources detected at 1415 MHz. The observation of the Coma Cluster (A 1656) has been fully reduced and the optical identification of the radio sources has been carried out. In this paper we present the data on sources identified with galaxies brighter than $m_p=17.5$, for all of which the measurement of the recession velocity has become available. The remaining part of the radio sources detected together with the results of an optical identification program will be published separately on the Supplement Series of this Journal.

The first deep radio study of this cluster was done by Willson (1970) at 408 and 1407 MHz with the Cambridge One mile Telescope (the 5C4 survey). He detected 13 cluster galaxies with $m_v<17$ within 1°.9 radius from the centre of the cluster at 408 KHz. He detected 4 of these also at 1407 MHz, where the survey was limited to 0°.5 radius due to the narrower primary beam at the higher frequency. Our survey of the same

central region at 1415 MHz (Papers I and II), thanks to the higher sensitivity of the instrument used, yielded 10 detections of cluster galaxies with $m_p \leqq 17$, of which 4 were not detected before. The survey described in this paper yields a total of 20 detections of cluster galaxies with $m_p \leqq 17.5$. Two galaxies detected at 1415 MHz were below the noise at 610 MHz. The total number of Coma galaxies identified with a radio source at one at least of the three frequencies, 408, 610 and 1415 MHz, amounts to 26.

The 20 galaxies detected in this survey are used in this paper to obtain the 610 MHz LF for this cluster, separately for the ellipticals and SO's, and the spirals and irregulars. Given the reasonable statistics achieved we then try a comparison of the LF of the galaxies in this cluster with that based on other samples (other clusters and field galaxies).

The two remarkable sources in the central region of Coma, 5C4.81 and 85, identified respectively with NGC 4869 and 4874, were the subject of a thorough discussion both by Willson (1970) and by Jaffe and Perola (1974). The new maps at 610 MHz of these two sources and the spectral index $\alpha_{610}^{1415}$ distribution along the tailed source 5C4.81 are presented and commented on. Finally we discuss the measurements of the extended low brightness source surrounding 5C4.81 and 85, which shows up in our map of the central region. This evidence confirms directly the conclusion reached by Willson (1970) that the "halo" source is *not* due to the contribution of discrete sources associated with galaxies in the rich cluster core.

The detection of new galaxies in Coma may also be important for the purpose of testing the statistical significance of the anomalous distribution in redshift found by Tifft and Tarenghi (1975a, see also Tifft, 1974) for the cluster galaxies detected in the 5C4 and in our 21 cm surveys with respect to the total sample of Coma galaxies for which the redshifts are known. This problem will not be discussed here but in a separate paper (Tifft and Tarenghi, in preparation).

In this paper we take the Hubble constant to be $100\,\mathrm{km\,s^{-1}\,Mpc^{-1}}$ and the distance to the cluster 69 Mpc.

## II. Observations

The operations of the WSRT are described in general in Högbom and Brouw (1974) and the specific techniques used for cluster surveys in Papers I and II. The details of the baselines, field centre, and hour angles observed at 610 MHz in Coma are given in Table 1. The field centre was identical to that used at 1415 MHz.

The instrument was calibrated by periodic observations of 3C48, 3C147 and 3C309.1. The assumed positions and fluxes of these sources are given in Table 2.

Table 1. Observation specifications. Field center: R.A. = $12^h56^m36^s.01$ (1950), Dec. = 28°11′42″.2 (1950)

| Observation date | Baseline coverage (m) | Hour angle coverage |
|---|---|---|
| 73265 | 54(72)1422 | −90° to −56° |
| 73249 | 54(72)1422 | −56 +16/+61 to +86 |
| 73264 | 54(72)1422 | +16 +33 |
| 73301 | 54(72)1422 | +86 +90 |
| 73229 | 72(72)1440 | −90 −77/−70 +90 |
| 73312 | 72(72)1440 | −77 −70 |
| 73241 | 90(72)1458 | −90 +08 |
| 73267 | 90(72)1458 | +08 +21 |
| 73240 | 90(72)1458 | +21 +24 |
| 73236 | 90(72)1458 | +24 +90 |
| 73320 | 108(72)1476 | −88 −74 |
| 73251 | 108(72)1476 | −74 +90 |

Notes: Date "73265" means 1973, sidereal day 265. Baseline Coverage "54(72)1422" means measurements from 54 m to 1422 m at 72 m intervals.

Table 2. Calibration sources

| Source name | R.A. (1950) | Dec. (1950) | $S_{610}$ (Jy) |
|---|---|---|---|
| 3C 48 | $01^h34^m49^s.827$ | +32°54′20″.63 | — |
| 3C 147 | 05 38 43.503 | 49 49 42.87 | 37.78 |
| 3C 309.1 | 14 58 56.664 | 71 52 11.17 | — |

The positions are taken from Ryle and Elsmore (1973). The quoted r.m.s. uncertainties in these positions are of the order of 0″.03, but they are all based on an assumed absolute position of $\beta$ Persei which is uncertain to about 0″.2. After calibration the estimated uncertainties in the gains of individual receivers is about 5%, in their phases about 4°, and in their baselines about 4 mm.

## III. Data Reduction

The observations listed in Table 1 were reduced as described in Paper I. The Fourier transform of the observations provided a synthesized beam whose FWHP is 53″ in R.A. and 113″ in Dec. The first two sidelobes have heights −5% and +3% of the central peak and are located 1.5 and 2.5 beamwidths away from it. The finite increments in baseline result in a strong elliptical grating ring with semiaxes 1°.56 in R.A. and 3°.3 in Dec. The useful field is limited to a circle with 1°.6 radius about the field centre due to the primary beam attenuation.

A search of the transformed map was made to find the position and flux of all strong point sources. These were then subtracted from the map so that their grating rings would not disturb searches for weaker sources. Then the field was researched. This process was repeated until all

Table 3

610 MHz radio sources identified with galaxies brighter than $m_p = 17.5$

| Name | α (1950.0) (h) (m) (s) | δ (1950.0) (°) (') (") | $S_{map}$ (mJy) | $S_{sky}$ (mJy) | $\alpha_{610}^{1415}$ | D Param.s | $\alpha_o-\alpha_r$ (") | $\delta_\delta-\delta_r$ (") | Pos.Err. (")x(") | IC | Galaxy Name | Gal Type | $m_p$ | V ($Kms^{-1}$) | Remarks |
|---|---|---|---|---|---|---|---|---|---|---|---|---|---|---|---|
| (1) | (2) | (3) | (4) | (5) | (6) | (7) | (8) | (9) | (10) | (11) | (12) | (13) | (14) | (15) | (16) |
| 1251 + 27W2 | 12 51 45.95 | 27 53 49.2 | 661.15 | 4407 | | | 5.3 | -1.0 | 2.3 x 3.2 | I | Anon | E | 17.5* | 25710 d | |
| (Coma A=5C4.19) | ± .08 | ±2.5 | | ±485 | | | | | | | | | | | |
| 1251 + 27W3 | 12 51 52.29 | 27 20 57.8 | 4.40 | 82.5 | | | 14.1 | -37.6 | 6.5 x13.4 | III | N4789 | E/SO | 13.3 | 8224 a | Bright star within 1σ |
| ⊢——(5C4.20) | .41 | 13.3 | | 9.9 | | | | | | | | | | | |
| 1252 + 28W7 | 12 52 58.38 | 28 4 15.5 | 4.95 | 13.1 | | | 18.2 | -8.2 | 5.8 x11.8 | I | Zw160-15 | E/SO | 15.5 | 7498 a | |
| | .36 | 11.6 | | 2.9 | | | | | | | | | | | |
| 1252 + 29W1 | 12 52 15.96 | 29 12 12.6 | 5.05 | 114.8 | | | -3.0 | 21.8 | 5.8 x11.8 | I | N4793 | Sc | 12.3 | 2388 a | |
| ⊢——(5C4.22) | .36 | 11.6 | | 6.2 | | | | | | | | | | | |
| 1253 + 27W6 | 12 53 40.42 | 27 57 7.5 | 6.05 | 12.2 | | | 4.7 | -13.9 | 5.1 x10.1 | I | Zw160-20 | I | 15.5 | 4982 a | |
| | .31 | 9.9 | | 2.2 | | | | | | | | | | | |
| 1254 + 27W1 | 12 54 58.89 | 27 46 10.8 | 115.95 | 182.0 | 1.37 | (16",41",0°) | 1.5 | -4.2 | 2.3 x 3.2 | II | N4839 | E | 13.6 | 7376 a | |
| ⊢——(5C4.51) | .08 | 2.5 | | 10.8 | .15 | | | | | | | | | | |
| 1254 + 27W4 | 12 54 17.90 | 27 27 14.2 | 26.35 | 88.5 | | $D_\delta$=146". | 2.3 | -17.3 | 2.4 x 3.6 | II | N4827 | E | 14.1 | 7455 a | |
| ⊢——(5C4.43) | .09 | 3.0 | | 9.2 | | | | | | | | | | | |
| 1255 + 27W1 | 12 55 29.34 | 27 53 18.0 | 4.80 | 5.9 | -.50 | | 3.6 | -6.0 | 5.9 x12.2 | I | Anon | E | 16* | 20256 a | |
| | .37 | 12.0 | | 1.2 | .31 | | | | | | | | | | |
| 1255 + 27W6 | 12 55 53.32 | 27 34 48.6 | 6.95 | 12.6 | | | 1.2 | .3 | 4.5 x 8.8 | I | Anon | I | 16* | 7478 a | |
| | .27 | 8.6 | | 2.0 | | | | | | | | | | | |
| 1255 + 28W3 | 12 55 32.20 | 28 19 51.8 | 12.65 | 13.9 | 1.53 | | 8.7 | .9 | 3.1 x 5.4 | I | Anon | I | 16* | 8151 a | |
| | .16 | 5.0 | | 1.2 | .28 | | | | | | | | | | |
| 1255 + 28W6 | 12 55 40.48 | 28 30 55.8 | 36.40 | 44.5 | .92 | | 3.2 | -11.4 | 2.3 x 3.2 | I | N4848 | I/S | 14.2 | 7271 a | |
| ⊢——(5C4.58) | .08 | 2.5 | | 2.2 | .10 | | | | | | | | | | |
| 1255 + 28W11 | 12 55 44.84 | 28 59 1.1 | 4.70 | 12.5 | | | -.3 | -20.1 | 6.2 x12.7 | I | Zw160-58 | I/S | 15.5 | 7674 a | |
| | .39 | 12.5 | | 2.8 | | | | | | | | | | | |
| 1256 + 27W5 | 12 56 9.61 | 27 31 56.6 | 4.40 | 8.5 | | | 8.6 | 6.0 | 6.5 x13.4 | I | Zw160-64 | I | 15.4 | 7425 c | near grating ring |
| | .41 | 13.3 | | 2.0 | | | | | | | | | | | |
| 1256 + 28W7 | 12 56 37.03 | 28 23 14.2 | 16.35 | 17.0 | .51 | | 3.8 | -8.0 | 2.8 x 4.5 | I | N4858 | SB | 15.5 | 9491 a | |
| | .13 | 4.0 | | 1.1 | .12 | | | | | | | | | | |
| 1256 + 28W9 | 12 56 56.5 | 28 10 40 | 1173 | 1175 | 1.14 | | 5.0 | 13.3 | | II | N4869 | E | 14.9 | 6801 a | tail source length tail 5.5' |
| ⊢——(5C4.81) | | | | 4 | | | | | | | | | | | |
| 1257 + 27W8 | 12 57 53.22 | 27 39 54.8 | 4.45 | 7.7 | | | 4.1 | 31 0 | 6.3 x13.2 | I | Zw160-82 | I | 15.6 | 10871 b | |
| | .40 | 13.0 | | 1.5 | | | | | | | | | | | |
| 1257 + 28W1 | 12 57 10.73 | 28 13 46.0 | 396.05 | 400.3 | .74 | (15",29",20°) | 7.8 | 1.6 | 2.4 x 3.6 | II | N4874 | E | 13.7 | 7180 a | |
| ⊢——(5C4.85) | .09 | 3.0 | | 5.2 | .06 | | | | | | | | | | |
| 1257 + 28W7 | 12 57 27.15 | 28 6 12.2 | 7.30 | 7.7 | .94 | $D_\alpha$=27" | -13.4 | -4.8 | 4.4 x 8.6 | II | RB60 | SO | 17.5* | 7895 a | A $19^m$ galaxy within 2σ |
| | .26 | 8.4 | | 1.6 | | | | | | | | | | | |
| 1258 + 27W6 | 12 58 9.43 | 27 54 19.3 | 4.35 | 5.8 | | | -8.0 | 3.8 | 6.5 x13.4 | I | Zw160-86 | I | 15.4 | 7508 c | |
| | .41 | 13.3 | | 1.4 | | | | | | | | | | | |
| 1258 + 28W3 | 12 58 13.51 | 28 19 32.5 | 27.50 | 33.7 | .59 | | .8 | 1.5 | 2.3 x 3.2 | I | IC4040 | I/Sc | 15.1 | 7644 a | |
| ⊢——(5C4.108) | .08 | 2.5 | | 1.8 | .10 | | | | | | | | | | |
| 1258 + 28W6 | 12 58 31.24 | 28 3 34.0 | 26.10 | 34.6 | .85 | | -18.6 | -4.0 | 2.3 x 3.2 | I | N4911 | Sc | 13.7 | 7898 a | |
| ⊢——(5C4.117) | .08 | 2.5 | | 2.1 | .20 | | | | | | | | | | |
| 1258 + 28W11 | 12 58 16.44 | 28 47 28.1 | 6.50 | 13.4 | | | -2.7 | -8.6 | 4.8 x 9.4 | I | Anon | I | 16* | 8970 a | |
| ⊢——(5C4.109) | .29 | 9.2 | | 2.8 | | | | | | | | | | | |
| 1258 + 28W12 | 12 58 18.93 | 28 40 59.6 | 8.65 | 15.1 | | | 7.1 | 6.5 | 3.9 x 7.4 | I | Anon | E | 17* | 6314 a | |
| ⊢——(5C4.113) | .22 | 7.1 | | 2.0 | | | | | | | | | | | |
| 1258 + 28W20 | 12 58 59.62 | 28 57 9.8 | 4.05 | 14.5 | | | 19.4 | -24.7 | 6.9 x14.4 | I | Zw160-98 | S | 15.3 | 8922 b | |
| | .44 | 14.3 | | 3.7 | | | | | | | | | | | |
| 1259 + 28W1 | 12 59 0.90 | 28 8 36.6 | 4.90 | 7.4 | | | 9.5 | 40.7 | 5.8 x11.8 | III | N4921 | S | 13.7 | 5331 a | |
| | .36 | 11.6 | | 1.6 | | | | | | | | | | | |
| 1259 + 28W5 | 12 59 32.90 | 28 16 34.2 | 5.10 | 9.6 | | | 4.8 | -6.8 | 5.8 x11.8 | I | N4927 | E | 14.8 | 7600 a | |
| | .36 | 11.6 | | 2.0 | | | | | | | | | | | |
| 1300 + 28W1 | 13 0 17.83 | 28 24 21.5 | 4.95 | 14.3 | | | -8.0 | -4.7 | 5.8 x11.8 | I | Anon | - | 17* | 43000 a | $18^m$ star within 2σ |

[a]) Tifft and Tarenghi (1975) and private communication ($V$ relative to Galactic Centre).
[b]) Gregory (1975) ($V$ relative to Galactic Centre).
[c]) Chincarini and Rood (1972a, b) ($V$ relative to Centre of Local Group).
[d]) Schmidt (1965) ($V$ relative to Galactic Centre).

The two low map flux sources 1252+28W7 and 1258+28W20 are classified as IC I, although slightly outside the 3σ ellipse. IC of 1255+28W6 and of 1258+28W6: read II instead of I. Spectral index of 1257+28W7: read >.94

sources stronger than 16.5 mJy map flux were subtracted and all sources above 4σ were detected. Here σ is the r.m.s. effective noise, which was determined to be 1.0 mJy by a gaussian fit to counts of weak intensity deflections in the map. Care was taken to avoid the inclusion of spurious radio sources caused by the intersection of weak grating rings.

## IV. Radio Source Parameters

Of the 185 sources detected in the search program 27 were identified with bright galaxies ($m_p \leqq 17.5$) as described in Section V below. For these sources, we determined the following parameters, contained in Table 3.

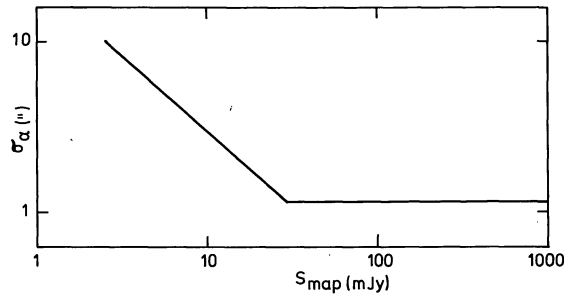


Fig. 1. The mean error in the measured R.A. of point or slightly resolved sources as a function of the map flux

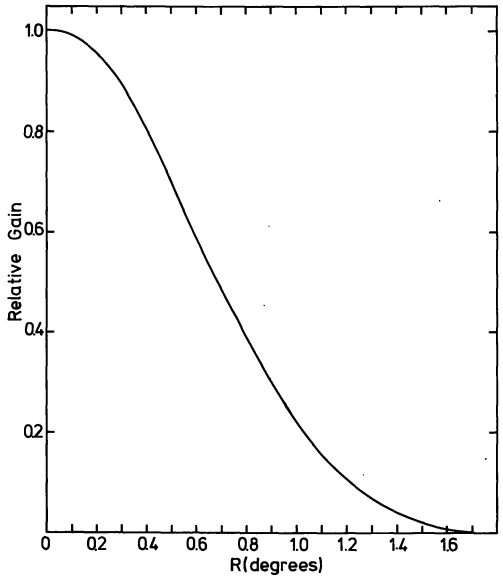


Fig. 2. The primary beam attenuation pattern

Column 1: Name of source.

Columns 2 and 3: 1950 positions and r.m.s. position errors. The errors are the mean of those found by the search program for sources of similar map flux density as explained in detail in Paper I. The good quality of this method in estimating these errors has been checked by comparing them to the differences in the radio positions determined by the search program in four independent full synthesis maps ($4 \times 12$ h each, at 1415 MHz) of a field studied with the WSRT by R.S. Le Poole, who kindly provided to us this information. Figure 1 shows the dependence of the error in R.A. on the map flux. Above a map flux of 28 mJy the random errors due to the noise are less than the systematic errors due to the uncertainties in the calibration procedures and the absolute positions of the calibrator sources. For sources stronger than this limit a constant error of 1.1″ in R.A. has been used. The errors in Dec. are larger than those in R.A. by a factor $\csc\delta$ or 2.15.

Column 4: Source map flux. This is the source flux uncorrected for the primary beam attenuation. For unresolved sources this is the flux found by a fit of the antenna pattern to the transformed intensities. For extended sources the flux was obtained during the estimate of the degree of extension (see below, Column 7).

Column 5: Sky flux and uncertainty. This is the map flux corrected for the primary beam attenuation, which is shown in Fig. 2. The errors quoted were obtained by combining the estimated errors in the map fluxes (taken to be 1.0 mJy for point sources and 1.5 mJy for slightly extended sources) and the error in the attenuation factor itself, which is estimated to be $10\,R\%$, where $R$ is the distance to the field centre in degrees. In addition there is an estimated 5% error in the absolute flux density scale.

Column 6: Spectral index. Given is $\alpha_{610}^{1415}$ for sources detected both in this and in the 1415 MHz survey (Paper I). The estimated uncertainty is also given.

Column 7: Extension parameters. The size of slightly resolved sources is specified by the $D$ parameters defined as in Paper I to be $D_\alpha = \pi^{-1}(A^{-1}\partial^2 A/\partial U^2)^{1/2}$ $(U=0, V=0)$, and $D_\delta = \pi^{-1}(A^{-1}\partial^2 A/\partial V^2)^{1/2}$ $(U=0, V=0)$, where $A$ is the visibility amplitude of the source for an interferometer with projected baselines (in wavelengths) of $U$ and $V$ in the R.A. and Dec. directions respectively. For a symmetrical double source $D_\alpha$ and $D_\delta$ are equal to the projected separation of the components on the R.A. and Dec. axes. These parameters were estimated by Fourier transforming an area around the source back to the UV plane and making a second order polynomial fit to the visibility function. Where only one of $D_\alpha$ or $D_\delta$ exceeded 2.5 times their estimated r.m.s. uncertainty the source was considered resolved in one direction and the appropriate $D$ parameter is given in Column 7. If both $D_\alpha$ and $D_\delta$ were significantly large, the cross derivative $\partial^2 A/\partial U \partial V$ was also determined and from these the position angle of the major axis and the $D$ parameters along and perpendicular to this axis were found. These are given by a 3-entry $D$ parameter in Column 7. For unresolved sources upper limits of 100″ $(S_{map}/\sigma)^{-1/2}$ and 215″ $(S_{map}/\sigma)^{-1/2}$ can be put on the extensions in the R.A. and Dec. directions respectively. For all resolved sources the total source flux was taken to be $A(U=0, V=0)$, found during the same polynomial fitting procedure as the $D$ parameters. The very extended source 5C4.81 was treated separately. Its structure is described in Section VII. Its flux was derived by integrating numerically the map within the zero contour.

## V. Optical Data

Optical identifications were made on a 48″ Palomar Schmidt IIIaJ plate (kindly lent to us by Bertola) using the $XY$ measuring machine of the ROUB group at Bologna. As in Paper I, we subdivide the identifications with bright galaxies in three classes. Class I identifications include the unresolved sources which satisfy the $3\sigma$ criterion:

$$\frac{(\Delta\alpha)^2}{\sigma_\alpha^2+\sigma_0^2}+\frac{(\Delta\delta)^2}{\sigma_\delta^2+\sigma_0^2}\leqq 9$$

where $\Delta\alpha$ and $\Delta\delta$ are the differences between the most probable radio position and the centre of the optical image of the galaxy. $\sigma_\alpha$ and $\sigma_\delta$ are the r.m.s. uncertainties in the radio position. $\sigma_0$ is the uncertainty in the position of the centre of the optical image: this is about 2″.
Class II identifications include two types: extended sources whose brightness peak meets the $3\sigma$ criterion; resolved and unresolved sources which do not satisfy this criterion, but lie well within the optical extension of the galaxy. Sources whose position falls outside the $3\sigma$ ellipse and on the edge of, or just outside the galaxy, are identifications of Class III.
On the basis of these identifications we have compiled in Table 3 the following information:
Columns 8 and 9: The differences between the optical and radio positions in R.A. and Dec.
Column 10: The r.m.s. combined radio and optical position errors in R.A. and Dec.
Column 11: Identification Class.
Column 12: Galaxy name in the catalogs. Zw stands for Zwicky and Herzog (1963) (called ZH thereafter); RB stands for Rood and Baum (1967).
Column 13: Morphological type of the galaxy. Adopted from Rood and Baum (1967) for the galaxies in their list, and from Gregory (1975) and Tifft and Tarenghi (private communication) for the others. Note in particular that the emission line galaxy identified with 1255+28W3, classified as Ep in Papers I and II, turned out to be a complex system, that in this paper is classified as an Irregular.
Column 14: Photographic magnitude. Taken from ZH if $m_p \leqq 15.7$, or estimated by the authors from the print of the Palomar Sky Survey O-plate. The latter magnitudes are indicated by an asterisk, and are uncertain by 0.2–0.5$^m$.
Column 15: Recession velocities. The references are given in the notes to the table.
Column 16: Remarks on radio structure and alternative identifications meeting the $3\sigma$ criterion.
The finding charts of all sources in Table 3, except those detected also at 1415 MHz (for these see Paper I), are reproduced in Fig. 3.
Not all the 27 galaxies listed in Table 3 belong to the Coma Cluster. We take as members those 22 whose recession velocity differs by less than $3\sigma_v$ from the cluster mean $\bar{V}$ ($\sigma_v = 900$ km s$^{-1}$ and $\bar{V} = 6900$ km s$^{-1}$, according to Rood *et al.*, 1972).
For a fraction of these 22 galaxies the identification could be due to a chance coincidence. In order to estimate the probable fraction, we have first counted the cluster galaxies with $m_p \leqq 15.7$ within a circle of 0°.48 radius about the radio field centre, and within a ring extending from 0°.48 to 1°.44 radius (using the redshifts listed in Gregory, 1975, to decide for the membership). We have subdivided the radio field in these two regions to take care in a rough way of the radial dependence of both the projected density of the galaxies in the cluster and of the density of detected radio sources. The latter is due to the shape of the primary beam attenuation pattern (Fig. 2). We have then estimated the number of cluster galaxies with $15.7 < m_p \leqq 17.5$ in the two regions by extrapolation, using the optical luminosity function of this cluster given by Abell (1962), assuming no mass segregation. The expected number of chance identifications meeting the $3\sigma$ criterion was obtained using the formula

$$N_{\text{c.i.}} = 9\pi \csc\delta \Sigma \sigma_\alpha^2 N_g / A$$

where $N_g$ is the number of galaxies counted in the area $A$, and the sum is extended to all sources detected in the survey within the same area. The results in Table 4 show that the expected number of spurious identifications is 1, while the number of Class I identifications, plus those of Class II meeting the $3\sigma$ criterion, amounts to 17. This makes us feel confident that at least 90% of the Class I and II identifications are real associations. On the other hand, the two cluster galaxies in Class III are probably identified by chance, and we shall not include them in the statistical analysis that follows.

## VI. The Radio Luminosity of the Coma Cluster Galaxies

We now use the 20 cluster galaxies detected to derive the radio luminosity function (LF) in Coma, i.e. the fraction of galaxies that are found to emit per interval of radio power. The so called bivariate LF (BLF) is obtained when this fraction is given as a function of the absolute optical magnitude also. It is important to derive the BLF, because it has been shown that the LF depends strongly on the optical luminosity of the galaxies, both inside and outside clusters (cf. Paper II). As in Paper II, we subdivide the galaxies in two groups, the elliptical and SO's, (E+SO), the spirals and irregulars, (S+I), and derive the LF separately for the two groups.
As explained in detail in Paper II, the area of the cluster and hence the number of galaxies surveyed at a given radio power increases with the power, due to the primary beam attenuation of the telescope. We have counted the cluster galaxies in circles of increasing radius about the radio field centre, and combined these counts with the attenuation pattern (Fig. 2) to yield the number of galaxies surveyed as a function of power plotted in Figs. 4 and 5. The cluster galaxies down to $m_p = 15.7$ (corresponding to $M_p = -18.4$) have been counted from the ZH Catalog. To decide for the membership and for the morphological classification we have followed Gregory (1975), who lists the redshift of all galaxies with $m_p \leqq 15.7$ within 2°.8 from the cluster centre, and classifies the galaxies on the basis of their image on glass copies of the Palomar Sky Survey. Due to

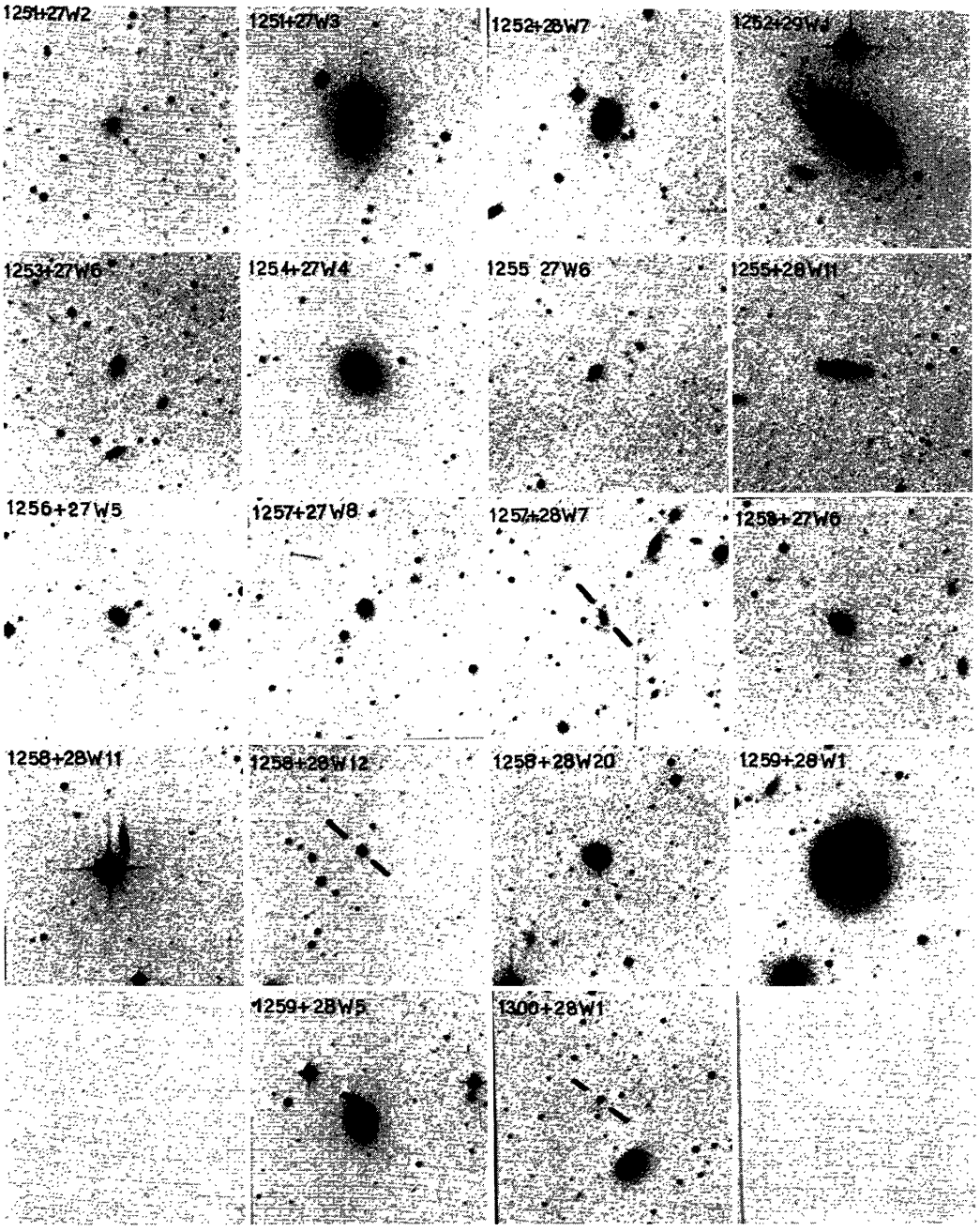


Fig. 3. Finding charts of all sources in Table 3, except those detected also at 1415 MHz (Paper I). North to the top, east to the left. Scale: 9.′3/mm

Table 4. Estimate of number of chance identifications

| Radius | Number of radio sources | $m_p$ | Number of galaxies | Expected chance ident. s | Number of identifications |
|---|---|---|---|---|---|
| 0 – 0.°48 | 45 | $m_p \leqq 15.7$ | 74 | 0.3 | 5 |
| | | $15.7 < m_p \leqq 17.5$ | 135 | 0.5 | 1 |
| 0.°48 – 1.°44 | 121 | $m_p \leqq 15.7$ | 84 | 0.2 | 8 |
| | | $15.7 < m_p \leqq 17.5$ | 150 | 0.3 | 3 |
| Total | 166 | | 443 | 1.3 | 17 |

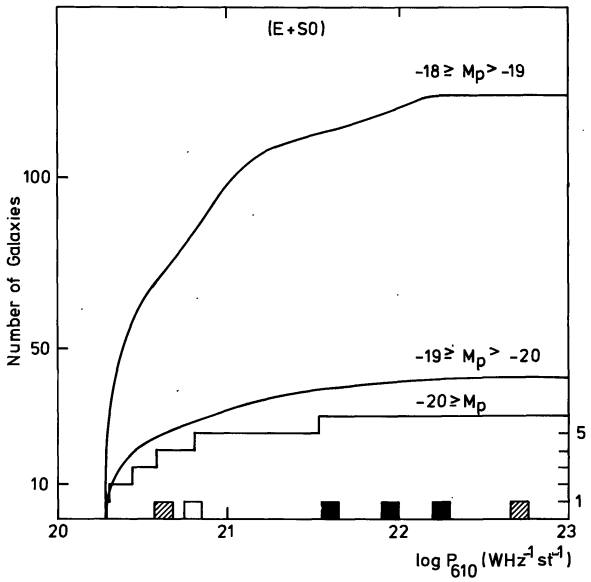


Fig. 4. The number of (E+SO) cluster galaxies surveyed, in three intervals of optical magnitude, as a function of radio power. The scale on the right side refers to the galaxies wiht $M_p \leqq -20$. The squares represent the detections (black: $M_p \leqq -20$; dashed: $-20 < M_p \leqq -19$; white: $-19 < M \leqq -18$)

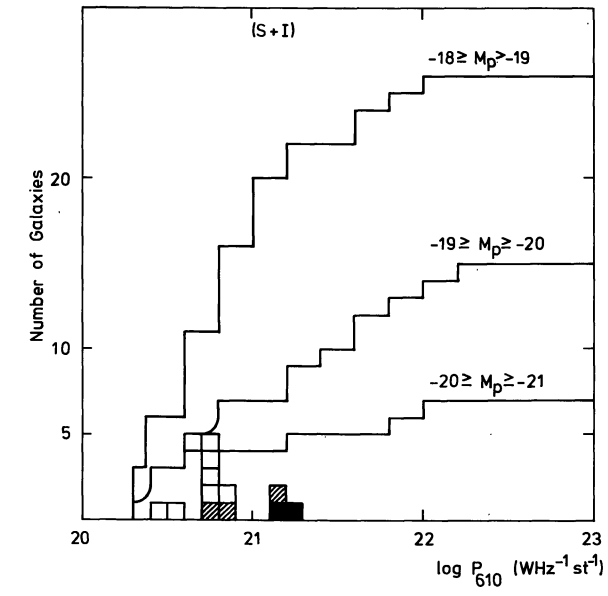


Fig. 5. The number of (S+I) cluster galaxies surveyed, in three intervals of optical magnitude, as a function of radio power. The squares represent the detections (black: $M_p \leqq -20$; dashed: $-20 M_p \leqq -19$; white: $-19 < M_p \leqq -18$)

the inadequacy of the material used, this classification is not very accurate, especially for "compact" spiral, which tend to be classified as SO's. This appears from a comparison with the classification by Rood and Baum (1967) based on 200″ plates of a more restricted area around the centre of Coma. The three misclassifications found this way are all spiral with a very blue color. For this reason we have included in the (S+I) group 8 galaxies classified by Gregory as intermediate between SO and S, and which appear blue in color on the Palomar Sky Survey print, none of which has been detected. Their contribution amounts to 25% of the total number of (S+I) galaxies surveyed. To the magnitude of the spiral galaxies we have applied a correction for internal absorption, using the relationship between the correction and the apparent axial ratio given by Holmberg (1958). For each galaxy we estimated the axial ratio on the Palomar Sky Survey print. The correction applied is very uncertain. On the other hand it cannot be ignored altogether, when the galaxies are subdivided in intervals of optical magnitude.

The number of surveyed galaxies fainter than $m_p = 15.7$ has been estimated by extrapolation, using the optical luminosity function given in Abell (1962) and assuming no mass segregation. For the (S+I) group, which contributes only 20% of the total below $15^m.7$ and for which the extrapolation may introduce a large error if its optical luminosity function were very different from that of the other group, we stopped at $m_p = 16.1$ ($M_p = -18$).

### *a)* LF *of the* (E+SO) *Galaxies*

The eight (E+SO) cluster galaxies detected are listed in Table 5a, along with the intrinsic radio power, the absolute photographic magnitude, the maximum physical extension or upper limits on it, the distance $R$ from the radio field centre, and a note on the presence of emission lines. The last information is from Tifft and Tarenghi (1975 and priv. commun.). Of the five used in Paper II to obtain the LF at 1415 MHz, 1256+28W8 was not detected in this survey, and 1255+28W3 is now classified in the (S+I) group. The bivariate LF is obtained from Fig. 4 and is tabulated in Table 6. In each bin the number of detections divided by the number of detectable galaxies is given. The monovariate LF (for galaxies with $M_p \leqq -17$) is also given. The "errors" quoted in this and the next tables are purely statistical. The upper (lower) error bounds represent the maximum (minimum) value the luminosity function may take for the probability of detecting less (more) galaxies than we actually did is greater than 16%. For the sake of comparing the Coma cluster LF with the combined LF obtained at 1415 MHz for 5 rich clusters (including Coma itself, see Paper II), we give at the bottom of Table 6 the integral values of the BLF above the minimum power detectable in this survey, $P_{610} = 2 \times 10^{20}$ WHz$^{-1}$ sterad$^{-1}$, in each interval of optical magnitude. The comparison with the corresponding values (assuming an average spectral index 0.7) at $P_{1415} = 10^{20}$ (Paper II, Fig. 3) shows no disagreement for the brightest class ($M_p \leqq -20$) of galaxies, but a deficiency of a factor about three with respect to the expectation value based on the 5 cluster sample for the

Table 5a. Sources identified with cluster elliptical or SO galaxies

| Source | Galaxy | $P_{610}(\times 10^{20})$ (WHz$^{-1}$ sterad$^{-1}$) | $M_p$ | $l_{r.a.}$ (kpc) | $l_{dec}$ (kpc) | $l_{max}$ (kpc) | $R$ (deg) | Notes |
|---|---|---|---|---|---|---|---|---|
| 1252+28W7 | Zw 160–15 | 5.9 | −18.7 | <15 | <32 | | .81 | No emission lines |
| 1254+27W1 | NGC 4839 | 82.4 | −20.6 | | | 14 | .56 | No emission lines normal continuum |
| 1254+27W4 | NGC 4827 | 40.1 | −20.1 | | | 49 | .90 | No emission lines normal continuum |
| 1256+28W9 | NGC 4869 | 532.3 | −19.3 | | | 110 | .08 | No emission lines normal continuum |
| 1257+28W1 | NGC 4874 | 181.3 | −20.5 | | | 10 | .13 | No emission lines normal continuum |
| 1257+28W7 | RB 60 | 3.5 | −16.7* | | | 9 | .21 | No emission lines |
| 1258+28W12 | Anon | 6.8 | −17.2* | <11 | <23 | | .62 | No emission lines normal continuum |
| 1259+28W5 | NGC 4927 | 4.3 | −19.4 | <15 | <32 | | .65 | No emission lines neutral color |

Table 5b. Sources indentified with cluster spiral and irregular galaxies

| Source | Galaxy | $P_{610}(\times 10^{20})$ (WHz$^{-1}$ sterad$^{-1}$) | $M_p$ | $l_{r.a.}$ (kpc) | $l_{dec}$ (kpc) | $R$ (deg) | Notes |
|---|---|---|---|---|---|---|---|
| 1253+27W6 | Zw 160–20 | 5.5 | −18.7 (−18.7) | <14 | <29 | .69 | Markarian 53 strong emission lines |
| 1255+27W6 | Anon | 5.7 | −18.2* (−18.2*) | <13 | <27 | .64 | Strong emission lines |
| 1255+28W3 | Anon | 6.3 | −18.2* (−18.2*) | < 9 | <20 | .27 | OII, OIII emission blue continuum |
| 1255+28W6 | NGC 4848 | 20.2 | −20.0 (−21.0) | < 5 | <12 | .38 | Complex emission blue continuum |
| 1255+28W11 | Zw 160–58 | 5.7 | −18.7 (−19.2) | <15 | <33 | .81 | Weak emission lines very blue |
| 1256+27W5 | Zw 160−64 | 3.9 | −18.8 (−18.8) | <16 | <34 | .67 | Markarian 56 emission lines |
| 1256+28W7 | NGC 4858 | 7.7 | −18.7 (−18.8) | < 8 | <18 | .99 | Complex emission |
| 1258+27W6 | Zw 160−86 | 2.6 | −18.8 (−18.8) | <16 | <34 | .45 | Emission lines very blue |
| 1258+28W3 | IC 4040 | 15.3 | −19.1 (−19.4) | < 6 | <14 | .38 | Emission lines slightly blue continuum |
| 1258+28W6 | NGC 4911 | 15.7 | −20.5 (−20.6) | < 7 | <14 | .45 | No emission lines normal continuum |
| 1258+28W11 | Anon | 6.1 | −18.2* (−19.2*) | <13 | <28 | .70 | Complex emission |
| 1258+28W20 | Zw 160−98 | 6.6 | −18.9 (−18.9) | <17 | <35 | .92 | Complex emission |

Table 6. Luminosity function of (E+SO) galaxies

| $\log P_{610}$ (WHz$^{-1}$ sterad$^{-1}$) | $-17 \geqq M_p > -18$ | $-18 \geqq M_p > -19$ | $-19 \geqq M_p > -20$ | $-20 \geqq M_p > -21$ | DLF (%) $M_p \leqq -17$ |
|---|---|---|---|---|---|
| 22.6 | 0/145 | 0/124 | 1/42 | 0/6 | $0.3^{+.3}_{-.1}$ |
| 22.2 | 0/145 | 0/124 | 0/42 | 1/6 | $0.3^{+.3}_{-.1}$ |
| 21.8 | 0/140 | 0/120 | 0/40 | 1/6 | $0.3^{+.3}_{-.1}$ |
| 21.4 | 0/132 | 0/113 | 0/38 | 1/6 | $0.3^{+.3}_{-.1}$ |
| 21.0 | 0/123 | 0/107 | 0/35 | 0/5 | ≦0.7 |
| 20.6 | 1/97 | 1/84 | 1/28 | 0/5 | $1.4^{+0.7}_{-0.5}$ |
| 20.2 | 0/64 | 0/54 | 0/17 | 0/2 | ≦1.4 |
| LF($\geqq 10^{20.2}$) (%) | $1.0^{+0.8}_{-0.3}$ | $1.2^{+0.9}_{-0.4}$ | $6^{+3.4}_{-1.3}$ | $50^{+23}_{-11}$ | |

Table 7. Luminosity function of (S+I) galaxies

| $\log P_{610}$ (WHz$^{-1}$ sterad$^{-1}$) | $-18 \geqq M_p > -19$ | $-19 \geqq M_p > -20$ | $-20 \geqq M_p > -21$ | DLF(%) $M_p \leqq -18$ | (a) | |
|---|---|---|---|---|---|---|
| 21.4 | 0/22 | 0/10 | 0/5 | $\leqq 4.8$ | | |
| 21.2 | 0/22 | 0/9 | 1/5 | $2.8^{+2.2}_{-0.8}$ | 1.9 | 0.8 |
| 21.0 | 0/20 | 1/7 | 1/4 | $6.4^{+4.2}_{-1.9}$ | 4.2 | 2.2 |
| 20.8 | 2/16 | 1/7 | 0/4 | $11^{+5.9}_{-3.7}$ | 7.0 | 4.1 |
| 20.6 | 3/11 | 1/5 | 0/4 | $20^{+10}_{-6}$ | 9.0 | 8.0 |
| 20.4 | 1/6 | 0/3 | 0/3 | $8.3^{+6.6}_{-2.5}$ | 10 | 9.1 |
| 20.2 | 0/3 | 0/1 | 0/1 | $\leqq 36$ | 12 | 15 |
| LF($\geqq 10^{20.2}$) (%) | $56^{+21}_{-11}$ | $49^{+23}_{-9}$ | $45^{+25}_{-10}$ | | | |

(a) Differential monovariate LF($M_p \leqq -18$) based on Cameron's sample of field spirals. The two entries refer to a different correction to the optical magnitudes used by Cameron (see text).

class $-20 < M_p \leqq -19$. This difference could be easily due to statistical fluctuations, since a large "error" affects both the expectation value and that obtained from the present sample.

### *b)* LF *of the* (S+I) *Galaxies*

The twelve (S+I) cluster galaxies detected are listed in Table 5b, similar to Table 5a. The information on the spectroscopic properties are from Tifft and Tarenghi (1975 and priv. commun.). The values of $M_p$ in brackets are corrected for internal absorption. Of the six detected at 21 cm, 1256+27W4 (RB 219) is missing because it is under the detection limit at 610 MHz. The LF in the bivariate and monovariate form is obtained from Fig. 5 and tabulated in Table 7. A LF of spirals that might be considered typical of rich clusters and be suitable for a comparison is not yet available, because of the very few detections obtained by us at 1415 MHz, except for Coma itself (cf. Paper II). The only significant comparison that can be made is with the radio properties of nearby spirals, for which the 408 MHz surveys of southern bright galaxies ($m_p \leqq 11$, $m_p \leqq 12.5$) by Cameron (1971a) can be used. Cameron's sample contains nearby spirals mostly in the "field" and some belonging to the "loose" cluster in Virgo. Cameron (1971b) shows that in the nearby spirals the radio and optical powers are correlated; the same property for the Coma spirals can be seen from Table 7, where the average radio power increases going from the interval ($-19 < M_p \leqq -18$) to the interval ($-21 < M_p \leqq -20$). For a quantitative comparison we use the MLF instead of the more relevant BLF, because we hope that the MLF is less sensitive to the fact that the magnitude scale adopted by Cameron (1971a) is not fully consistent with that used by ZH. Comparison of Cameron's photomagnitudes, with his "aperture" correction removed, with those of ZH for the bright galaxies in common ($m_p \simeq 11$) shows that the ZH magnitudes are on the average $0^m.6$ fainter, with an r.m.s. deviation of $0^m.6$. It is not clear, however, that the average difference for galaxies of $14$–$15^m$, like those in the cluster sample, would be the same. For this reason we have derived the two values of the LF for the "field" spirals given in the last Column of Table 7. For the first we used Cameron's magnitudes corrected for internal absorption, but without the "aperture" correction. For the second we simply added $0^m.6$ to all magnitudes used in the first derivation. The 408 MHz fluxes were reduced to 610 MHz using a spectral index of 0.7. Since the optical luminosity distribution of the spirals in the nearby sample is very different from that of the spirals in our sample (mostly due to the selection effects which

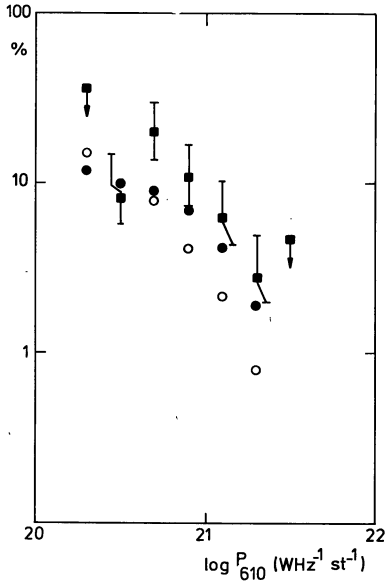


Fig. 6. The differential luminosity function of the cluster (S+I) galaxies with $M_p \leqq -18$ (■). The black and white circles represent the luminosity function of "field" spirals with $M_p \leqq -18$, based on the survey by Cameron (1972a, b) with and without the $0^m.6$ correction (see text)

are usual in optically complete samples like that in Cameron, 1971a), the two values given in Table 7 have been adjusted to represent the MLF of the "field" spirals, as if they had the same optical luminosity distribution of the spirals surveyed in Coma. The two values are given without the statistical "errors", since they are much smaller than those from our sample, and the uncertainty due to the magnitude system used is in fact larger than the statistical one. The MLF's are plotted in Fig. 6. Confirming the result obtained at 1415 MHz on the basis of only 5 detections (Paper II), the spirals in Coma appear to be slightly overluminous as compared to the "field" spirals. The difference would be larger, if we did not include in the (S+I) group the eight blue galaxies whose morphological type is rather dubious. However, because of the uncertainty on the optical magnitudes and, to a lesser extent, on the morphological classification of the cluster galaxies, this result should still be considered marginally significant.

### c) *Radial Dependence of the* LF

To examine whether the probability of radio emission for a galaxy depends on the radial distance from the cluster centre, we have subdivided the field surveyed into an "inner" region, within 30′ from the radio field centre (which is 12′ away from the cluster centre), and an "outer" region, and compared the LF in the two regions. Due to the limited number of detections, a comparison in each interval of optical magnitude would be insignificant. On the other hand the value of a monovariate LF is very sensitive to the optical luminosity distribution of the galaxies in a sample. Therefore the MLF of the outer region has been obtained after adjusting the slightly different luminosity distribution to match that of the inner region. The values of the MLF ($M_p \leqq -18$), integrated down to the lowest power detectable in the outer region, $P = 2.6 \times 10^{20}$ WHz$^{-1}$ sterad$^{-1}$, are presented in Table 8. The values found are consistent with the independence of the LF from the radial distance from the cluster centre.

We note that the two most powerful ellipticals are situated in the inner region, although the optically brightest galaxies ($M_p \leqq -19$) are equally numerous in the two regions. This kind of separation is not apparent among the spirals.

Table 8. The values (%) of the integral monovariate LF ($M_p \leqq -18$, $P_{610} \geqq 2.6 \times 10^{20}$) for the "inner" and "outer" regions

| | <30′ | >30′ |
|---|---|---|
| (E+SO) | $3^{+2}_{-1}$ | $7 \pm ^{4}_{2}$ |
| (S+I) | $50^{+25}_{-15}$ | $31 \pm 13$ |

## VII. Other Properties of the Detected Cluster Galaxies

### a) *Spectral Indexes*

The spectral indexes $\alpha_{610}^{1415}$ of the radioemitting galaxies detected both at 1415 and 610 MHz are given in Table 3. Two sources found in the 1415 MHz survey and identified with cluster galaxies (Papers I and II) were not detected at 610 MHz, according to the $4\sigma$ criterion in Section III. For the source 1256+27W4 (identified with the SBa galaxy RB219) we found a $3\sigma$ deflection at the position of the 1415 MHz source, which yields an index of −0.06. For 1256+28W8 (identified with the E galaxy N 4865) we use a $3\sigma$ upper limit on its $S_{610}$ to obtain an upper limit on the index of 0.0. All the galaxies detected at 610 MHz within the 0°.6 radius of the field surveyed at 1415 MHz were detected also at the other frequency except RB60. The spectral indexes of the 4(E+SO) galaxies detected in both surveys range from 0.74 to 1.37, and those of the 5 (S+I) galaxies range from 0.51 to 1.53. These values are similar to those found in other galaxies for various ranges of radio power (cf., for instance, Colla *et al.*, 1975). For the two galaxies N 4865 and RB 219 the negative value of the spectral index, a feature typical of compact nuclear sources, probably indicates that the radio source is selfabsorbed. This is consistent with the fact that no evidence of extension for these two sources was found at 1415 MHz.

### b) *Emission Lines*

The information on the presence of emission lines compiled in Tables 5a and 5b has been obtained in a homogeneous way by Tifft and Tarenghi (1975 and priv. commun.). None of the (E+SO) galaxies detected show evidence of emission lines. On the contrary 90% of the (S+I) galaxies detected have emission lines in their spectra at various degrees of intensity and complexity. For comparison we have used a recent compilation (Gregory and Tifft, 1975) of the redshifts of all Coma galaxies with $m_p \leqq 15.7$, where the presence of emission lines is registered. More information about the spectra of the (S+I) galaxies covered in the present survey has been kindly provided to us by W.G. Tifft. Limited to the area surveyed, the percentage of emission lines in the (E+SO) galaxies is 4%, in the (S+I) galaxies is 50 or 65% depending on whether the eight blue galaxies of dubious morphology are included in this group or not. The higher proportion of emission lines found among the (S+I) galaxies with radio power above the limit of this survey does indicate the probable existence of a correlation between the strength of the radio emission and the presence of emission lines.

Finally we point out that of the six Markarian galaxies (Markarian, 1967) in our field of view, two cluster members (irregulars with emission lines) have been detected, with a radio power close to the average of the (S+I) group.

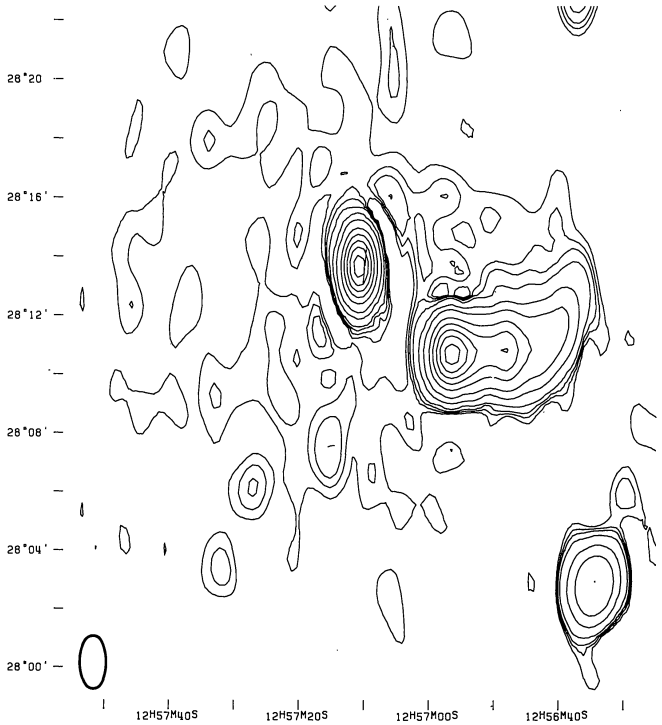


Fig. 7a. The 610 MHz map of the central region of the cluster. The slightly extended source near to the centre of the map is 5 C4.85. The tailed source to the right in 5 C4.81. The low brightness contours surrounding these two sources are due to the "halo" source Coma C. The source in the lower right corner is 1256+28W4ab (5C4.7ab), an optically unidentified double (see Paper I). The three contours source in the lower left quadrant is 1257+28W7 (see Table 3). The contours are: 2, 4, 6, 10, 25, 50, 100, ..., 300 mJy per synthesized beam. The beam, shown by the ellipse in the lower left corner, covers a solid angle of $1.25 \times 10^{-7}$ sterad

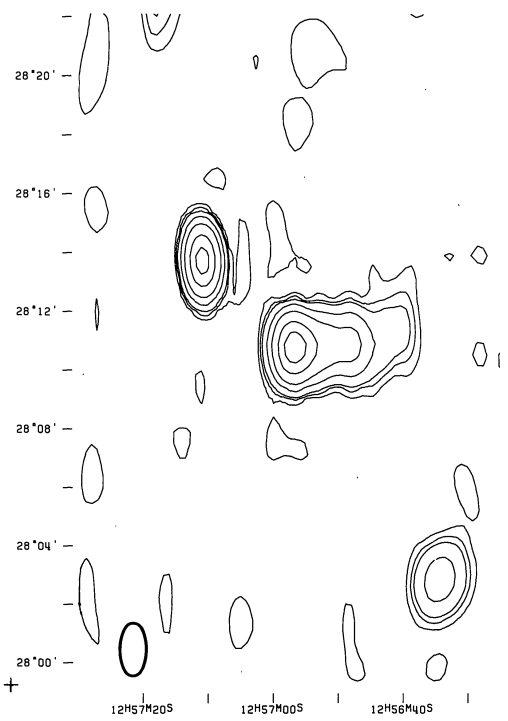


Fig. 7b. The 1415 MHz map of the same region as in Fig. 7a, with the beam convolved to the 610 MHz resolution. The contours are: 2, 6, 10, 25, 50, 100, 150 mJy per synthesized beam

## VIII. The Central Radio Sources

The 610 MHz observations give interesting new information on the structure of the sources 5C4.81, 5C4.85 and of the extended "halo" source. In earlier low resolution measurements this complex of sources was called Coma C; *here we will reserve this name for the "halo" source alone.* The three sources were first described and discussed in detail by Willson (1970). The WSRT observations of the first two at 1415 and 5000 MHz were presented and discussed in Jaffe and Perola (1974). The 610 MHz map of the central region of the cluster is shown in Fig. 7a. For comparison the earlier 1415 MHz WSRT observations convolved to the 610 MHz beam are shown in Fig. 7b. The maps at the two frequencies have been "cleaned" to remove the effects of sidelobes.

### *a)* 5C4.85 = NGC 4874

The 5000 MHz observations (Jaffe and Perola, 1974) show that this source is a double with a separation of 15″ and P.A. 30° and the 1415 MHz observations are consistent with this. The 610 MHz map shows a greater extension, as can be immediately seen by comparing the maps in Figs. 7a and 7b. The extension, estimated with the method described in Section IV, is 29″ along P.A. 20°. The spectral index $\alpha_{610}^{1415} = 0.74 \pm .06$ is larger than $\alpha_{1415}^{5000} = 0.49 \pm .2$, although the difference could be due to the uncertainty on the 5000 MHz measurement[1]). The data indicate that beside the double sources there is a more extended component, whose spectrum must be steeper than about 1.2 to explain the absence of any noticeable beam broadening in the 1415 MHz map convolved. The extension of 29″ quoted above is the root mean square of the sizes of the double and of the larger component weighted according to their flux. To find the size of the larger component we need to assume a value for its relative contribution to the total flux. Assuming that the spectral index of the double is constant and equal to the measured $\alpha_{1415}^{5000}$, the excess of 70 mJy at 610 MHz can be attributed to the other component, whose size then turns out to be 60″. If on the other hand its flux were smaller, its extension must be larger to yield the observed beam broadening, although presumably not larger than the beam width itself or about 2′ in declination, otherwise we would see the two components separately.

[1]) The flux measured by Willson (1970) at 408, $S_{408} = 406$ mJy is surprisingly close to the $S_{610}$ measured with the WSRT. This is probably due to a difference in the calibration procedure rather than to a real flattening of the spectrum, since also the Cambridge flux at 1407 MHz is lower than the WSRT $S_{1415}$ (Jaffe and Perola, 1974), yielding a spectral index $\alpha_{408}^{1407} = 0.74$, equal to our $\alpha_{610}^{1415}$.

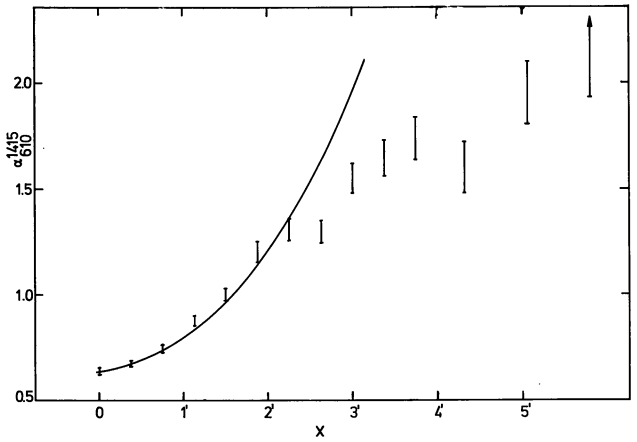


Fig. 8. The spectral index $\alpha_{610}^{1415}$ along the tail of 5C4.81. The curve represents the prediction of the model discussed in Jaffe and Perola (1974), with $V_g = 1500\ \mathrm{km\ s^{-1}}$ and $B = 14\ \mu\mathrm{G}$

The steepness of the spectrum suggests that this component is the remnant of activity that took place previous to the generation of the compact double. The near coincidence in P.A. of its elongation and of the axis of the double suggests that the direction along which the radio events developed did not vary markedly with time. There are several other examples of this kind, like 3C236 (Willis *et al.*, 1974) and 3C84 (Miley and Perola, 1975).

*b)* 5C4.81 = NGC 4869

This is one of the head-tail sources, and on the 610 MHz map the tail is seen to extend about 3′ straight to the West, then curve up rather sharply to the NW and extend about 3′ farther before disappearing into Coma C. The spectral index steepens along the tail, typical of head-tail sources. In Fig. 8 we plot $\alpha_{610}^{1415}$ along the tail; the index is computed from the ratio of the 610 MHz map to the convolved 1415 MHz map. This curve agrees reasonably with the run of $\alpha_{408}^{1407}$ given by Willson (1970) although in the first 1′ of the tail our spectral index is about 0.1 flatter than his. The difference arises probably from the "cleaning" procedure applied to our map and from the apparent slight mismatch between his 408 MHz beam and his convolved 1407 MHz beam.

The run of the spectral index $\alpha_{1415}^{5000}$ in the first 2′ of the tail was discussed in Jaffe and Perola (1974), under the hypothesis that the tail is due to the motion of the parent galaxy through the intracluster medium. There it was found that the change in spectral index could be explained if the electrons were accelerated in the "head" region and suffered only radiative losses thereafter, provided that the magnetic field in the tail were equal the equipartition value of $14\,h^{2/7}\ \mu G^2$), and the galaxy velocity in the plane of the sky were $1500\,h^{-4/7}\ \mathrm{km\ s^{-1}}$.

However the prediction of this model on the run of $\alpha_{610}^{1415}$ farther along the tail lies considerably above the measured points, as can be seen in Fig. 8. To match the data would require a velocity of about $2000\,h^{-4/7}$ $\mathrm{km\ s^{-1}}$, or a magnetic field of $11\,h^{2/7}\ \mu G$. Such a velocity is not excessive for a cluster galaxy, but it makes it more difficult to explain the low value of the observed radial velocity of $-173\ \mathrm{km\ s^{-1}}$ (Rood *et al.*, 1972) with respect to the cluster average. The lower value of the magnetic field is a more plausible alternative.

This is one of several cases where this explanation of the spectral index rise in head-tail sources can be made to work only by taking a plausible but somewhat improbable value for the velocity (e.g. Vallée and Wilson, 1976). This might imply either that the electrons are accelerated also in the tail, or that they are provided also by an external source.

The bend in the tail is rather sharp, having a projected radius of curvature of 2′ or about $40\,h^{-1}$ kpc. At about the same place where the bending begins, an extended region of low surface brightness becomes visible on the North side of the tail, which is weak or absent on the South side. There is an indication that the spectral index of this region is steeper by at least 0.3 than at the centre of the tail, although there is about a 5% chance that this result is due to a noise fluctuation. One explanation of these effects is that the galaxy is travelling on a curved orbit through the cluster, presumably with a focus somewhere between NGC 4874 and the other central giant elliptical NGC 4886. If the orbit is circular its radius equals the distance from the focus to the point of maximum curvature in the tail, or about $10' = 200\,h^{-1}$ kpc. Then the sharpness of the bend could be explained by projection effects if the inclination of the orbital plane to the plane of the sky is about 70°. It may also be that the inclination is less, but that the bend is at the apicentre of a highly eccentric orbit. The weak northern extension may represent a part of the tail "around the bend" which is projected on top of a later part of the tail. If the curvature is indeed gravitational, there must be sufficient mass within the orbital radius to produce the bending. The virial mass of the whole cluster has been estimated as $3 \times 10^{15}\ M_\odot$ (Rood *et al.*, 1972) and, from the mass distribution model of King (1972) about 8% of this, or $2 \times 10^{14}\ M_\odot$ lies within 200 kpc of the centre. This is adequate to hold NGC 4869 on such a circular orbit if its velocity is near the 1500 to 2000 $\mathrm{km\ s^{-1}}$ inferred from the spectral data.

Another explanation of the curvature which has been discussed in the literature is buoyant lifting of the tail in the cluster gravitational field (Cowie and McKee, 1975), in which case the low brightness area might be sign of a breakup of the tail due to the Kelvin-Helmholtz instability. However the tail curves toward the cluster centre and not away from it, which in this case would require a non-radially symmetric mass distribution in the cluster.

[2]) h is the Hubble constant in units of $100\ \mathrm{km\ s^{-1}\ Mpc^{-1}}$.

*c) Coma* C

The existence of a very extended (~40′), steep spectrum radio source in Coma was deduced by Willson from the fact that the contribution of the discrete sources in the 5 C 4 interferometric survey could not account for the flux measured from the cluster on low resolution, single dish surveys. Our detection of Coma C simultaneously with the discrete sources confirms his interpretation. The source can be seen clearly in the radiophoto in Fig. 9 and in the contour map in Fig. 7a, where the contours are broken up by noise and remnant side lobes from other sources. We cannot estimate directly the extent and flux of the source from these maps because even on our shortest baseline, 54 m, it is strongly resolved. By assuming a particular model of the source brightness distribution, however, we can extrapolate the source visibility amplitude down to zero interferometric spacing and estimate the flux under this assumed distribution.

The short baseline measurements were affected by solar and television interference of up to 5 Jy. Those measurements disturbed by solar interference were omitted from further analysis. The television interference (TVI) rotates rapidly in phase relative to the source signal and can be weakened by averaging the measured complex visibility function over periods of 1 h. The reamining TVI was of the order of 200 mJy. We have attempted to reduce this further by assuming that the TVI was totally polarized, and Coma C totally unpolarized. The strength of the TVI could then be determined from the $Q$, $U$ and $V$ Stokes parameters measured by the crossed dipole receivers and this strength removed from the observations.

In Fig. 10 we plot the logarithm of the corrected visibility amplitude of Coma C as a function of the square of the baseline projected on the sky. These measurements come entirely from the shortest (54 m) measured baseline, where, because of the viewing geometry, the projected baseline varies from 27 m to 54 m during the observation. Because of solar interference, only hour angles from $-63°$ to $+3°$ are included in this plot. The measured points lie on a fairly smooth curve; the scatter is only large on the longest projected baseline, where it is partly due to noise.

It the source brightness distribution is circularly symmetric and gaussian, i.e. proportional to $\exp(-R^2/2a^2)$ where $R$ is the distance from the cluster centre, then $\log S$ as plotted in Fig. 10 should be a linear function of the square of the baseline $L$. Given the uncertainties in the interference correction, and in the assumption of circular symmetry, we find a straight line fit in Fig. 10 adequate, and this yields $a = 12' \pm 2'$ on the sky, where the uncertainty comes from the variation in slope along the measured points. If the distribution is in fact gaussian then extrapolation of the curve to zero baseline gives the total flux to be 4 Jy with an uncertainty of about 1.5 Jy.

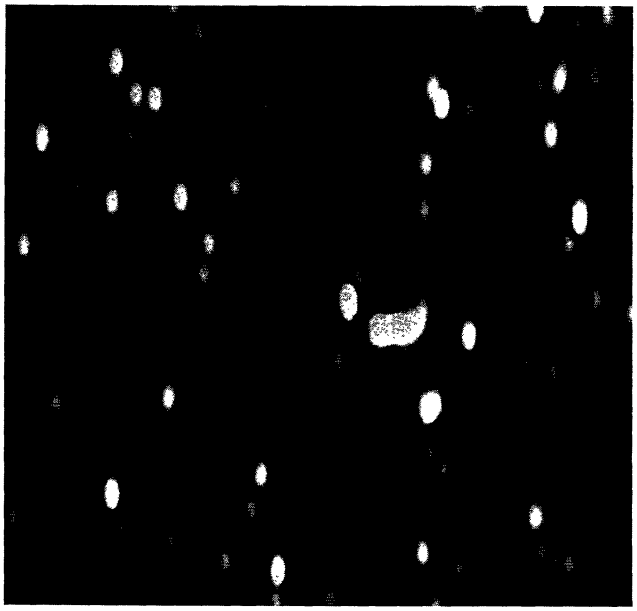

Fig. 9. A photographic reproduction of the 610 MHz map of an area $1° \times 1°$ about the cluster centre. Notice the low brightness "halo" source, ~30′ across, around the two bright central sources. Noise and remnant sidelobes of these two sources are the main causes of the features that can be discerned in it. The majority of the other sources in this map are background

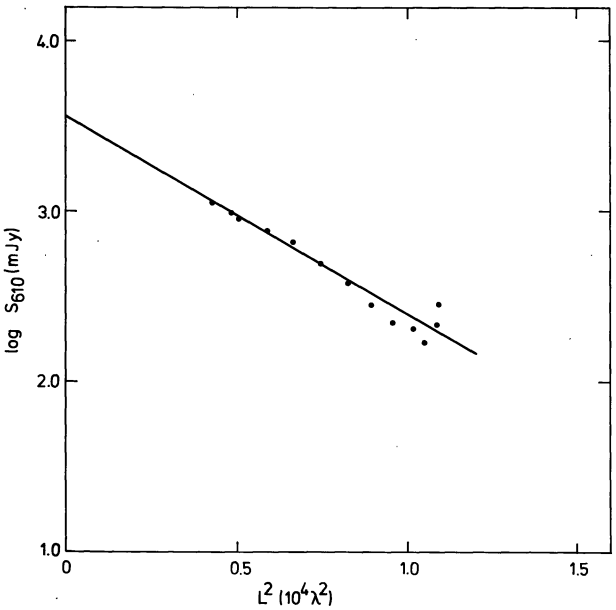


Fig. 10. The dots represent the corrected visibility amplitude of Coma C as a function of the square of the baseline projected on the sky. The straight line fit corresponds to a gaussian circularly symmetric brightness distribution

The flux agrees with that derived by Willson (1970) from the single dish measurements of Bozyan (1968) and from extrapolation from lower frequencies. The radius is somewhat smaller than those found from lower frequency measurements (Willson, 1970) although these were made with instruments of rather poor resolution, in most case $\gtrsim 40'$. If there is in fact a decrease in size with increasing frequency, it could be interpreted as due

to shorter radiative lifetime of the electrons emitting at 610 MHz with respect to those emitting at lower frequencies, if the electrons were diffusing toward the outer part of the cluster from a centrally located injection source (or sources).

The source radius is also marginally smaller than that found for the X-ray source in Coma. A value of $a = 16' \pm 3'$ was found by Lea *et al.* (1973), but their fit to the X-ray data assumed an emissivity proportional to $(r^2 + a^2)^{-3}$, which gives rise to a brightness distribution as a function of $R$ incompatible with the visibility function in Fig. 10, so that the two values of the source radius are not directly comparable.

As seen in Figs. 7a and 9 the centroid of the observed brightness lies near to the centre of the cluster, which is about 2′ East of 5C4.85, rather than near the field centre of the observation, slightly West of the head of 5C4.81, as we would have expected if its appearance were strongly affected by interference. The reality of small scale features seen in Fig. 7a is dubious since they may be produced by noise, sidelobes of discrete sources, or by the remaining TVI.

*Acknowledgements.* The authors thank Prof. W. G. Tifft, Drs. Tarenghi and Gregory for the information kindly provided in advance of publication, Prof. F. Bertola for the plate used to identify the sources, and the Bologna Group, ROUB, for the help in the identification programme. G.C.P. acknowledges financial support from the Italian Consiglio Nazionale delle Ricerche. The Westerbork Radio Observatory and Reduction Group are administered by the Netherlands Foundation for Radio Astronomy (S.R.Z.M.) with the financial support of the Netherlands Organization for Pure Research (Z.W.O.).

## References

Abell, G.O. 1962, in *Problems of Extragalactic Research*, G.C. McVittie Ed., Macmillan, N. Y.
Bozyan, E.P. 1968, *Astrophys. J.* **152**, L 155
Cameron, M.J. 1971a, *Monthly Notices Roy. Astron. Soc.* **152**, 403
Cameron, M.J. 1971b, *Monthly Notices Roy. Astron. Soc.* **152**, 429
Chincarini, G., Rood, H.J. 1972a, *Publ. Astron. Soc. Pacific* **84**, 589
Chincarini, G., Rood, H.J. 1972b, *Astron. J.* **77**, 4
Colla, G., Fanti, C., Fanti, R., Gioia, I., Lari, C., Lequeux, J., Lucas, R., Ulrich, M.H. 1975, *Astron. & Astrophys.* **38**, 209
Cowie, L.L., McKee, C.F., 1975, *Astron. & Astrophys.* **43**, 337
Gregory, S.A. 1975, *Astrophys. J.* **199**, 1
Högbom, J.A., Brouw, W.N. 1974, *Astron. & Astrophys.* **33**, 289
Holmberg, E. 1958, *Meddn. Lund. Astron. Ser.* II, No. 136
Jaffe, W.J., Perola, G.C. 1974, *Astron. & Astrophys.* **31**, 223
Jaffe, W.J., Perola, G.C. 1975, (Paper I), *Astron. & Astrophys. Suppl.* **21**, 137
Jaffe, W.J., Perola, G.C. 1976, (Paper II), *Astron. & Astrophys.* **46**, 275
King, I.R. 1972, *Astrophys. J.* **174**, L 123
Lea, S.M., Silk, J., Kellogg, E.M., Murray, S. 1973, *Astrophys. J.* **184**, L 105
Markarian, B.E. 1967, *Astrofizica* **3**, 55
Miley, G.K., Perola, G.C. 1975, *Astron. & Astrophys.*, **45**, 223
Rood, H.J., Baum, W.A. 1967, *Astron. J.* **72**, 398
Rood, H.J., Page, T.L., Kintner, E.C., King, I.R. 1972, *Astrophys. J.* **175**, 627
Ryle, M., Elsmore, B. 1973, *Monthly Notices Roy. Astron. Soc.* **164** 223
Schmidt, M. 1965, *Astrophys. J.* **141**, 1
Tifft, W.G., Gregory, S.A. 1975, Direct Observations of the Large Scale Distribution of Galaxies, preprint
Tifft, W.G., Tarenghi, M. 1975, *Astrophys. J.* **199**, 10
Tifft, W.G. 1974, IAU Symp. n. 58, *The Formation and Dynamics of Galaxies*, D. Reidel Pub. Co. pg 239
Vallée, J.P., Wilson, A.S. 1976, *Nature* **259**, 451
Willis, A.G., Strom, R.G., Wilson, A.S. 1975, *Nature* **250**, 625
Willson, M.A.G. 1970, *Monthly Notices Roy. Astron. Soc.* **151**, 1
Zwicky, F., Herzog, E. 1963, Catalogue of Galaxies and of Clusters of Galaxies, Vol. 2, Calif. Inst. of Technology, Pasadena

W. J. Jaffe
Institute for Advanced Study
Princeton, N. J. 08540, USA

G. C. Perola
Istituto di Scienze Fisiche
Via Celoria, 16
I-20133 Milano, Italy

E. A. Valentijn
Sterrewacht
Leiden 2405, The Netherlands